Electrochimica Acta 135 (2014) 284–292

Contents lists available at ScienceDirect

Electrochimica Acta

journal homepage: www.elsevier.com/locate/electacta

Photoanodes with mesoporous TiO_2 beads and nanoparticles for enhanced performance of CdS/CdSe quantum dot co-sensitized solar cells

Ru Zhou[a,b], Qifeng Zhang[a], Evan Uchaker[a], Lin Yang[a], Naiqiang Yin[b], Yonghu Chen[b], Min Yin[b], Guozhong Cao[a,*]

[a] Department of Materials Science and Engineering, University of Washington, Seattle, WA 98195, USA
[b] Department of Physics, University of Science and Technology of China, Hefei 230026, China

ARTICLE INFO

Article history:
Received 26 February 2014
Received in revised form 15 April 2014
Accepted 5 May 2014
Available online 14 May 2014

Keywords:
quantum dot sensitized solar cell
photoanode
mesoporous TiO_2 bead
surface area
light scattering

ABSTRACT

Photoanode is a critically important component in quantum dot sensitized solar cell (QDSC), and its configuration will exert a tremendous influence on the cell performance. In this paper, submicrometer-sized mesoporous TiO_2 beads were prepared for QDSC application in view of their high specific surface area, superior light scattering and easy electrolyte penetration. Two configurations for the photoanodes were designed and studied with mesoporous TiO_2 beads combined with nanoparticles: a double-layer configuration composed of a thick bead layer on top of a thin nanoparticle layer, and a mixture structure made of mixed mesoporous TiO_2 beads and nanoparticles. Photovoltaic results showed that double-layer and mixture configurations delivered power conversion efficiencies of 4.33% and 4.65%, respectively, achieving impressive improvement compared to the single-layer films made from mesoporous beads or nanoparticles (~4%). The mesoporous TiO_2 beads served as scattering layer or scattering centers to enhance light scattering and boost the photocurrent while the incorporation of nanoparticles into the voids between mesoporous beads further increased the surface area for QD loading and led to better connection between the neighboring beads. Electrochemical impedance spectroscopy analysis revealed a retarded charge recombination for the mesoporous beads when combined with nanoparticles, reflected in the increase of open circuit voltage.

1. Introduction

There is a strong demand for the development of low-cost and high-performance solar devices as clean and sustainable energy partially to replace fossil fuels [1]. Quantum dot-sensitized solar cells (QDSCs) as a derivative of dye-sensitized solar cells (DSCs) have attracted considerable attention in recent years [1–5]. QDSCs are relatively cost-effective and easy to manufacture. Compared to organic dyes, narrow band gap semiconductor QDs possess versatile extraordinary optical and electrical properties in terms of (1) tunable band gap across a wide energy range, (2) strong light absorption, (3) high stability against oxidative deterioration, (4) high extinction coefficients and (5) large intrinsic dipole moment facilitating charge separation [6–11]. A high theoretical photovoltaic conversion efficiency up to 44% in view of the multiple excitation generation (MEG) effect has encouraged people to develop QDSCs with the use of various QDs [12], such as CdS [2,9–11,13,14], CdSe [2,9–11,15,16], CdTe [17], PbS [18], and Ag_2S QDs [19], as sensitizers for light harvesting. However, the power conversion efficiency of the QDSC up to now, typically around 1~5%, still lags far behind the record power conversion efficiency of 15%, reported recently for DSCs [20]. Therefore, efforts are still urgently needed to boost the efficiency of QDSC and explore its full potential.

Aside from the QD sensitizer, the photoanode configuration as a critically important part of QDSC drastically impacts the cell performance. It is of great importance to have the photoanode structure for high QD loading, strong light scattering, efficient electron transport and quick electrolyte diffusion [21]. The mesoporous TiO_2 nanoparticle films (for example, commercial P25 nanoparticle) have been extensively studied as the photoanodes for QDSCs and DSCs, due to the appreciable internal surface area and good electron transport [2,22–24]. However, typical nanometer-sized TiO_2 particles (≈20 nm) in the photoanodes are very weak scatters in the generation of light scattering because the size of the

* Corresponding author. Tel.: +1206 616 9084; fax: +1 206 543 3100.
E-mail address: gzcao@u.washington.edu (G. Cao).

http://dx.doi.org/10.1016/j.electacta.2014.05.021
0013-4686/

nanoparticles is far smaller than the wavelengths of visible light, resulting in a significant portion of the light emitted on the phtoanodes transmitting through the film without interacting with the sensitizer [25,26]. According to the Mie theory and Anderson localization of light [27,28], resonant scattering of light is predicted to occur for spherical particles, when the particle size is comparable to the wavelengths of incident light. A strong scattering effect would extend the distance that light travels within the photoanode film, provide the photons with more opportunities to be absorbed by sensitizers (i.e., dye molecules or QDs), and thus eventually enhance the light-harvesting capability of the photoanode. As a result, submicrometer-sized mesoporous sphere was considered to be a promising material for DSC or QDSC in view of their high specific surface area and strong light scattering effect [29–31]. Scattering centers and scattering layers have been effectively employed to enhance light harvesting for improved cell performance. Ferber et al. suggested the use of 250∼300 nm TiO_2 particles as the scattering centers mixed in a TiO_2 matrix consisting of 20 nm particles [32]. Wang et al. employed a mixture of 23 nm particles and 100 nm particles to fabricate a photoanode for DSC application, and achieved a higher efficiency (8.4%) than the photoanode made from only 23 nm particles (7.6%) [33]. However, it is evident that the introduction of large particles as scattering centers would reduce the dye/QD loading capacity of the photoanode. As for the more favorable way of utilizing an upper scattering layer to enhance the light scattering, although significant effect has been reported in many cases [34–36], the commonly used scattering layer itself, such as a thin layer composed of 400 nm rutile TiO_2 or ZrO_2, does not produce much photocurrent due to very low surface area. Furthermore, the thickening of film thickness further increases the transport distance of the photon-generated electrons which in turn leads to high charge recombination rate in the solar cell [21,37].

Compared to the extensive research of the mesoporous beads as scattering centers or scattering layers in DSC, there is relatively little systematic and in-depth study on such beads for QDSC application. In our previous work [38], submicrometer-sized mesoporous TiO_2 beads were demonstrated to be good candidates for QDSC application in view of high specific surface area, effective light scattering and easy electrolyte penetration. However, for the photoanode consisting of TiO_2 beads only, the large voids exist between the submicrometer-sized mesoporous beads result in a loss of internal surface area, insufficient connection between adjacent beads, and poor contact between TiO_2 film and FTO substrate. The combination of mesoporous TiO_2 beads and nanoparticles is expected to increase the surface area for more QD sensitizers and facilitate the charge transfer in the photoanode, while retaining light scattering effect. The present study is aimed to optimize the photoanode configuration for QDSC through the combined use of mesoporous TiO_2 beads and nanoparticles. The designed photoanodes, i.e., double-layer and mixture configurations, address the drawbacks of single-layer film made of TiO_2 beads or nanoparticles, and demonstrate the improvement in the cell performance.

2. Experimental

2.1. Synthesis of Mesoporous TiO_2 beads

Mesoporous TiO_2 beads were prepared from a two-step method combined precipitation and solvothermal process [31,39]. Firstly, amorphous precursor beads were prepared via a precipitation process in the presence of hexadecylamine (HAD, 90%, Sigma-Aldrich) as structure-directing agent and KCl to control the monodispersity of the precursor beads by adjusting the ionic strength of the solution. 5.296 g HAD was dissolved in 800 mL ethanol, followed by the addition of 3.20 mL KCl aqueous solution (0.1 M). To this solution, 17.6 mL titanium (IV) isopropoxide (TIP, 97%, Sigma-Aldrich) was added under vigorous stirring at ambient temperature. The resulting white TiO_2 suspension was kept static at the same temperature for 18 h, and then centrifuged. The beads were washed with ethanol three times and dried in air at room temperature. Secondly, to prepare mesoporous TiO_2 beads with a highly crystalline framework, a solvothermal treatment of the air-dried precursor beads was performed. Specifically, 0.96 g of amorphous precursor beads was dispersed in a 12 mL ethanol and 6 mL deionized water mixture with 25% ammonia solution of 1 mL. Then the resulting mixture was sealed within a 30 mL antoclave and heated at 160 °C for 16 h. After centrifugation and ethanol washing, the air-dried powders were calcined at 500 °C for 2 h in air to remove organic residuals, resulting in the formation of mesoporous TiO_2 beads.

2.2. Preparation of photoanode films

To prepare the QDSC photoanode films, 0.5 g of solvothermally treated TiO_2 beads (or commercial P25 nanoparticles) mixed with 0.25 g ethylcellulose and 1.75 g α-terpineol were first dispersed into 5.0 mL ethanol, and then sonicated for 30 min to form a slurry after removing the ethanol under stirring. These procedures allowed the ethylcellulose to penetrate and intersperse between TiO_2 microspheres or nanoparticles. For the mixture TiO_2 paste, beads (0.25 g) and nanoparticles (0.25 g) with weight ratio of 1:1 were employed, followed by the same procedures as stated above. Finally, the doctor blade technique was employed to coat the resulting slurry on FTO glass substrates (∼3 mm in thickness, 27 Ω/square), and then the films were sintered at 500 °C for 30 min in air with a heating rate of 5 °C/min. The thickness of the TiO_2 films, measured from the cross sectional image of SEM, was ∼17 μm. The active area of the TiO_2 films was approximately 0.36 cm^2 (0.6 cm × 0.6 cm square).

2.3. Fabrication of CdS/CdSe QDs co-sensitized photoanodes

For the growth of CdS QDs, the TiO_2 films were first immersed into 0.1 M cadmium acetate ($Cd(CH_3COO)_2$) methanol solution for 1 min, rinsed them with methanol and dried in air. Successively, the films were dipped into 0.1 M sodium sulfide (Na_2S) solution mixed with water and methanol (1/1, volume ratio) for another 1 min to allow S^{2-} to react with the pre-adsorbed Cd^{2+}, leading to the formation of CdS QDs. Then, the electrodes were again rinsed with methanol and dried. The two-step dipping procedure is termed as one successive ionic layer absorption and reaction (SILAR) cycle. Four cycles were employed to obtain a suitable amount of CdS QDs on the films. The CdS QDs layer serves as a seeding layer facilitating the subsequent CdSe QDs growth. As for the CdSe QDs deposited on the CdS-coated TiO_2 films, a chemical bath deposition (CBD) method was employed. Briefly, 0.1 M sodium selenosulphate (Na_2SeSO_3) aqueous solution, 0.1 M $Cd(CH_3COO)_2$ aqueous solution, and 0.2 M trisodium salt of nitrilotriacetic acid ($N(CH_2COONa)_3$) solution were mixed together with a volume ratio of 1:1:1. Then the CdS-coated TiO_2 films were vertically immersed into the solution for the deposition of a CdSe layer under dark condition at 24 °C for 3 h. After the deposition of CdSe, a ZnS passivation layer was deposited by dipping alternatively into 0.1 M zinc acetate ($Zn(CH_3COO)_2$) and 0.1 M Na_2S solutions for 1 min/dip with two SILAR cycles. The deposition of ZnS is to improve the stability of the photoanodes.

2.4. Preparation of electrolyte and counter electrodes

The polysulfide electrolyte employed in this study was composed of 1 M S and 1 M Na_2S in de-ionized water. The counter electrode was a Cu_2S film fabricated on the brass foil. The

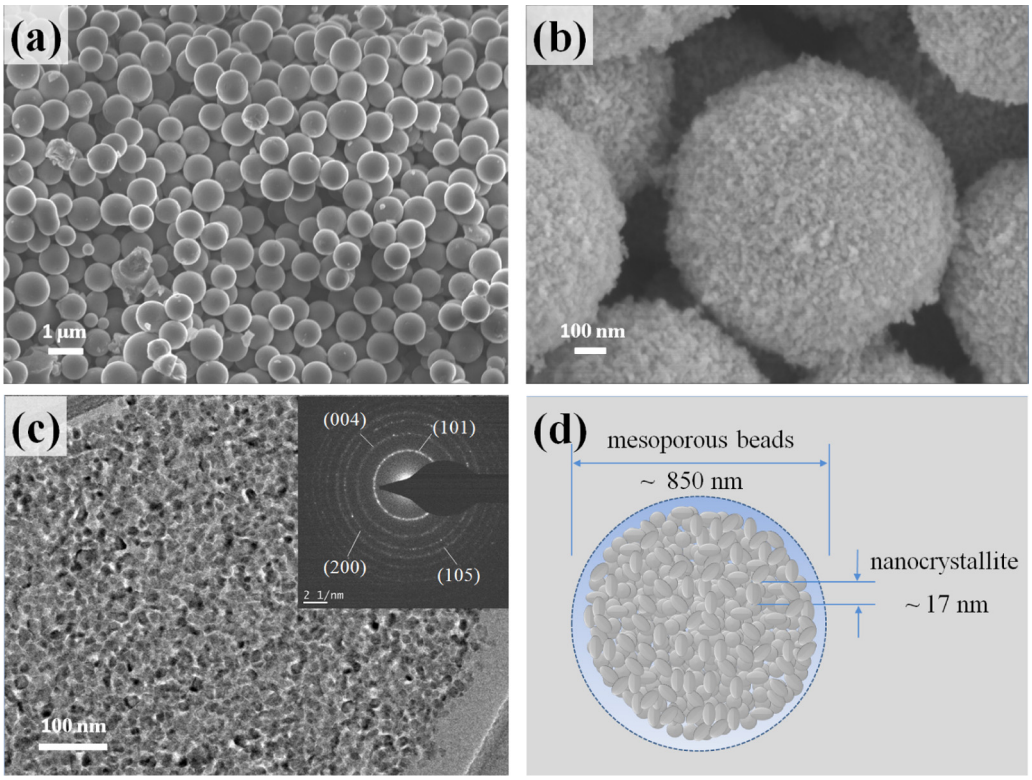

Fig. 1. SEM micrographs of (a) as-prepared precursor materials and (b) calcined mesoporous TiO_2 beads [38], (c) TEM image of the ultramicrotomed TiO_2 bead, and the inset shows the SAED pattern, and (d) a schematic diagram that illustrates the microstructure of TiO_2 beads comprising packed nanocrystallites.

preparation process of the Cu_2S electrode can be described as follows: brass foil was immersed into 37% hydrochloric acid (HCl) solution at about 70 °C for 30 min, then rinsed with water and dried in air. After that, the etched brass foil was dipped into 1 M S and 1 M Na_2S aqueous solution (the electrolyte) for about 5 min, resulting in a black Cu_2S layer forming on the foil. The solar cells were prepared by sandwiching a Cu_2S counter electrode and a QD-sensitized photoanode using a scotch tape spacer (~50 um in thickness) and permeating with the polysulfide electrolyte.

2.5. Characterization of materials and QDSCs

Morphology of the samples was characterized by a scanning electron microscope (SEM, JSM-7000) equipped with energy dispersion X-ray (EDX) used to analyze the element contents and distribution, and transmission electron microscopy (TEM, Tecnai G2 F20). X-Ray Diffraction (Bruker F8 Focus Powder XRD with Cu *K*α radiation) was used to verify the crystal phase and estimate the crystal size of the mesoporous TiO_2 beads. The diffractometer was set at 40 kV working voltage and 40 mA tube current, scanned from 20-80° at a rate of 0.02° s^{-1}. Nitrogen adsorption-desorption isotherms were measured using a Quantach-rome NOVA 4200e system, with samples degassed at 250 °C overnight under vacuum before tests. The multi-point Brunauer–Emmett-Teller (BET) method was used to calculate the specific surface area. A thermal scientific UV–Vis–NIR spectrophotometer (Evolution 300 PC) fitted with an integrating sphere accessory was employed for the analysis of reflectance properties of the TiO_2 films. The photovoltaic properties were measured using an HP 4155A programmable semiconductor parameter analyzer under AM 1.5 simulated sunlight with the power density of 100 mW/cm^2. The electrochemical impedance spectroscopy (EIS) was carried out through the Solartron 1287A coupling with the Solartron 1260 FRA/impedance analyzer to investigate electronic and ionic processes in QDSCs.

3. Results and discussion

Fig. 1a shows the morphology of the as-prepared microsphere precursors, the surfaces of which were quite smooth without noticeable pores or crystalline features. The precursor beads were amorphous and possessed a small specific surface area of 2.64 m^2/g based on our previous work [38]. Here it is important to indicate that some data about the beads in the present paper are from Ref. 38, as the same beads materials were employed. We will label the reference in the Figure Captions when the picture or figure curves from the previous work are used. After hydrothermal crystallization, rough surfaces and connected mesopores have emerged in the microspheres, as shown in Fig. 1b, and these mesoporous beads were ~850 nm in diameter on average, exhibiting a little polydisperse. The TEM image (Fig. 1c) shows that the beads were composed of packed TiO_2 nanocrystallites and interconnected mesopores, which opened a possibility of facile dye/QDs deposition into the inner part of mesoporous beads. The distinct selected area electron diffraction (SAED) pattern shown in the inset indicated a highly crystalline framework of TiO_2 with anatase phase. High-resolution TEM image (Fig. S1) also allowed the identification of the lattice fringes with *d*-spacing 0.352 nm correlated to the (101) planes of the anatase TiO_2. The schematic geometrical structure of the beads is illustrated in Fig. 1d, which demonstrates the mesoporous features provided by the aggregation of elongated TiO_2 nanocrystallites with the estimated average size of ~17 nm as displayed in TEM iamge.

Fig. 2a compares the XRD patterns of the mesoporous TiO_2 beads and commercial TiO_2 nanoparticles (Degussa P25). The mesoporous beads exhibited well-resolved diffraction peaks of the anatase TiO_2, while the pattern of P25 nanoparticles showed both anatase and

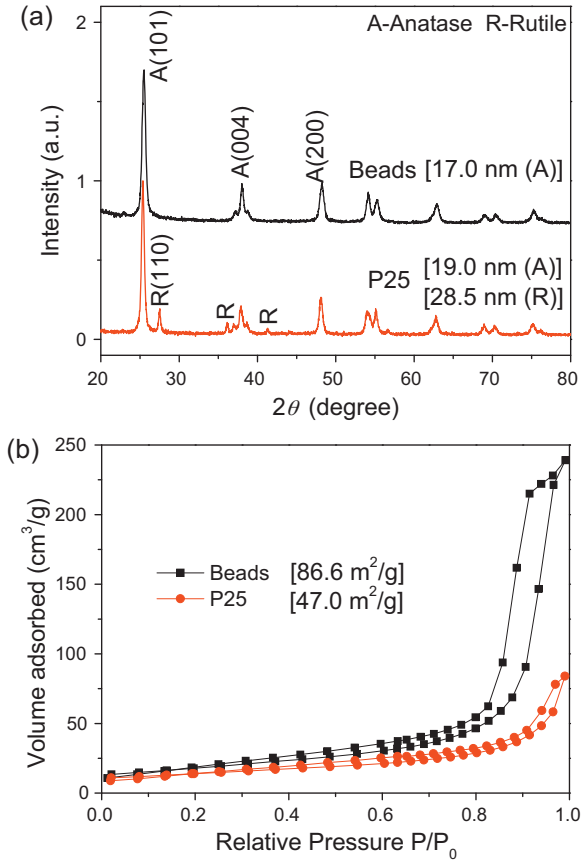

Fig. 2. (a) XRD patterns and (b) Nitrogen sorption isotherms of mesoporous TiO_2 beads [38] and P25 nanoparticles.

rutile phases. The corresponding crystal sizes are estimated by applying the Scherrer equation to the broadened (101) anatase and (110) rutile peaks. As shown in Fig. 2a, the anatase TiO_2 nanocrystallites in the beads revealed a crystal size of ~17 nm, close to the size of the P25 nanoparticles with anatase phase, however, much smaller than of the size of rutile TiO_2 as large as ~29 nm. It is known that the larger particle size will lead to a lower surface area, and this is consistent with the typical nitrogen sorption isotherms of the mesoporous beads and P25 nanoparticles as shown in Fig. 2b. The BET surface area of mesoporous beads (86.6 m^2/g) was almost two times that of P25 nanoparticles (47.0 m^2/g), clearly suggesting that extremely high specific surface areas were built into these mesoporous spherical structures. Type IV isotherm with H1 type hysteresis loop at relative pressures P/P_0 = 0.8-0.9 was observed for mesoporous beads, indicating the presence of large mesopores [31,40]. A mean diameter of 21.0 nm has been obtained for the mesopores in the beads, very close to the values reported in the literatures [31,40]. In order to evaluate the difference in the surface area between the films made from mesoporous beads and P25 nanoparticles, a dye-unloading experiment was further explored (Fig. S2). The result implied that the dye loading ability (or specific surface area) of the beads film was about two times that of nanoparticles film. Similar results has also been reported by Chen et al. [31].

Fig. 3a and b show the surface morphologies of the photoanode films made from mesoporous TiO_2 beads and P25 nanoparticles. It was found that the spherical morphology of the mesoporous beads was well preserved in the construction of the photoanodes and bound together after the sintering process; no obvious pulverization was observed. These results indicated that the as-prepared TiO_2 beads was constructed of interconnected nanocrystallites with

Table 1
Atom ratio of the elements measured by EDX on the surfaces of photoanode films made from mesoporous beads and P25 nanoparticles.

Photoanode	Cd, at%	Se, at%	S, at%	Zn, at%	Ti, at%	O, at%
Beads	9.70	5.48	5.45	1.80	24.93	52.64
P25	7.29	5.01	3.90	1.70	28.27	53.84

strong interaction forces between adjacent particles, giving rise to a robust mesoporous structure. This feature is of great importance in view of practical applications of these TiO_2 beads, as the ultrasonic treatment is commonly used for the preparation of TiO_2 paste or slurry. The large voids displayed among the beads on the film indicate a "open structure" of the photoanode, which has been suggested to facilitate the diffusion of the electrolyte within the film [41]. The "highway" provided by these large voids allows fast diffusion of the electrolyte throughout the thick TiO_2 layer. Furthermore, the internal pores with the diameter of ~21 nm in the beads also seems to be resonable for electrolyte diffusion as the diffusion distance in the beads is very short. In contrast, a compact film surface was revealed by P25 photoanode consisting of TiO_2 nanoparticle. A measurement of the ion diffusion constants performed by Kim et al. revealed that the hierarchical TiO_2 pore structure really induced relatively more efficient diffusion of the electrolyte compared with the dispersed nanoparticles [41].

Fig. 3c and d showed EDX spectra of two sensitized photoanodes indicated the successful deposition of CdS, CdSe, and ZnS. The atom ratios of the elements, listed in Table 1, revealed that the CdS, CdSe, and ZnS amount loaded onto the beads film was higher than that of P25 film. The mapping images of Cd element along the cross-section are shown in Fig. 3e and f (see Fig. S3 for the mapping images of S and Se elements). It can be seen that, Cd element presented a uniform and homogenous distribution in both of the photoanodes. The higher concentration of Cd element in the beads film further confirmed stronger QD loading ability of the mesoporous TiO_2 beads than that of P25 TiO_2 nanoparticles. As it is well known that the QD loading amount is closely related to the specific surface area of TiO_2, the mesoporous TiO_2 beads film is expected to allow higher QD loading in view of the higher surface area of the beads compared to that of P25 nanoparticles. However, considering the relatively small amount of TiO_2 employed in the beads film due to the large voids formation and the certain challenge of the formation of QDs in the innermost part of the beads, the QD amount loaded onto the beads film was only a little larger than that for P25 film, not simply proportional to the specific surface area of the TiO_2 (the BET surface area of mesoporous beads was about two times that of P25 nanoparticles).

Four groups of photoanode films were prepared for QDSC application in this study: (a) a single-layer of mesoporous TiO_2 beads, (b) a single-layer of standard Degussa P25 TiO_2 nanoparticles, (c) a double-layer configuration composed of a ~10 μm beads layer on top of a ~7 μm P25 layer, and (d) a single-layer of the mixture of beads and P25 nanoparticles (weight ratio≈1/1). Fig. 4 displays the cross section SEM images of the four photoanodes with the same thickness ~17 μm. Obviously, the two layers in the double-layer configuration (Fig. 4c) were in conformal attachment with no sign of delamination, and the mixture structure (Fig. 4d) also allowed the filling of the nanoparticles in the voids existed between the mesoporous beads.

For the mesoporous beads structure shown in Fig. 4a, the strong light scattering of the beads with large surface area significantly enhances the photon capturing capability of the film. However, the large voids between submicrometer-sized mesoporous beads could be filled, at least partially, to increase the accessible surface area to load more QD sensitizers, and the incompact connections between adjacent mesoporous beads and poor contact between TiO_2 film

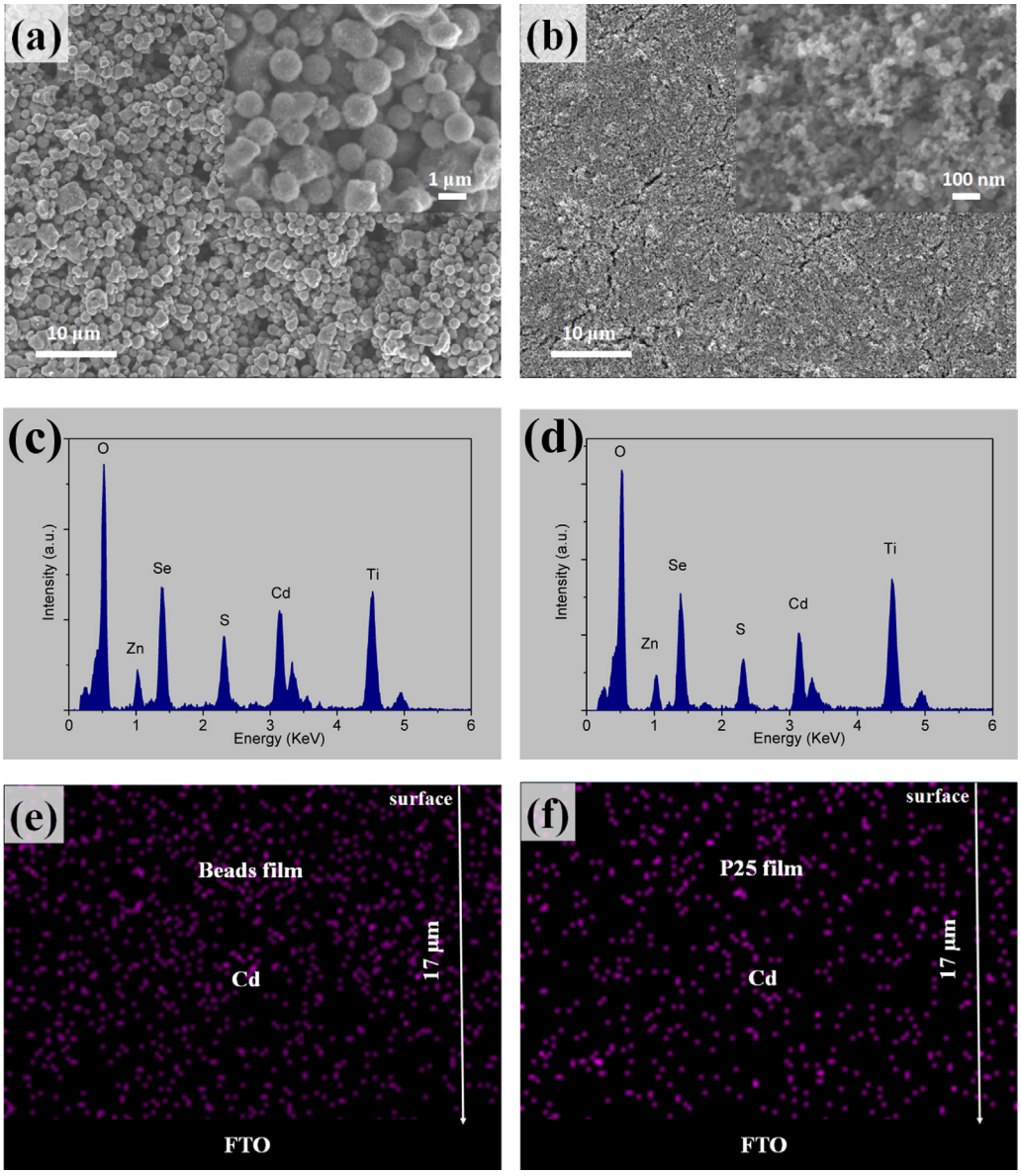

Fig. 3. SEM images of (a) the surface of mesoporous beads film and (b) the surface of P25 nanoparticle film, EDX spectra of CdS/CdSe QDs co-sensitized (c) mesoporous beads film and (d) P25 nanoparticle film, and EDX mapping images of Cd elements along the cross-section of (e) mesoporous beads film and (f) P25 nanoparticle film.

and the FTO substrate might also been improved for charge transfer through the incorporation individually dispersed TiO_2 nanoparticles [41,42]. The TiO_2 nanoparticle film (Fig. 4b) has been widely used in DSCs or QDSCs because of its appreciable surface area and good electron transport, but the high transparency and negligible light scattering due to the small particle size will result in poor light harvesting, as previously discussed. Therefore, both single-layer configurations made of TiO_2 beads or nanoparticles need further optimization for high efficiency QDSCs.

Two configurations of the photoanode via combined use of the mesoporous TiO_2 beads and nanoparticles were fabricated for QDSC application. The double-layer structure, as shown in Fig. 4c, is different from that in conventional double-layer DSC/QDSC, including a 12 μm thick nanoparticle film serving as an active layer covered by a 4 μm thick light scattering layer comprised of ~400 nm particles (i.e., a "12 μm + 4 μm" mode) [36]. In the double-layer structure here, the active layer is the mesoporous beads instead of the nanoparticles, as such, to maximize the benefits of mesoporous beads to QDSCs in terms of high surface area and strong light scattering. The bottom nanoparticles layer thinner than the top beads layer is proposed to absorb the light reflected by the mesoporous beads. Such a double-layer structured photoanode has a "7 μm + 10 μm" mode and is consistent with the optimal double-layer structure to maximize light harvesting suggested by Zhang et al. [21]. As illustrated in the schematic of Fig. 5a, the low reflectance of bottom nanoparticle layer should allow the passage of unabsorbed light into the upper beads layer, and the remarkable diffuse reflection in the beads layer significantly extends the traveling distance of light within the photoanode film and thus increases the opportunities for incident photons to be captured by the sensitizer. The light reflected back by the beads can be effectively utilized by the nanoparticle layer between the FTO and beads film. A photon-localization effect may also occur on these films when the light scattering is confined in closed loops. As for the mixture structure consisting of the mixed mesoporous beads and TiO_2 nanoparticles shown in Fig. 4d, submicrometer-sized mesoporous beads introduce the light scattering centers without sacrificing the accessible surface area for QD loading compared to the conventional scatters with low surface area. The incorporation of P25 nanoparticles makes full use of the large voids between the

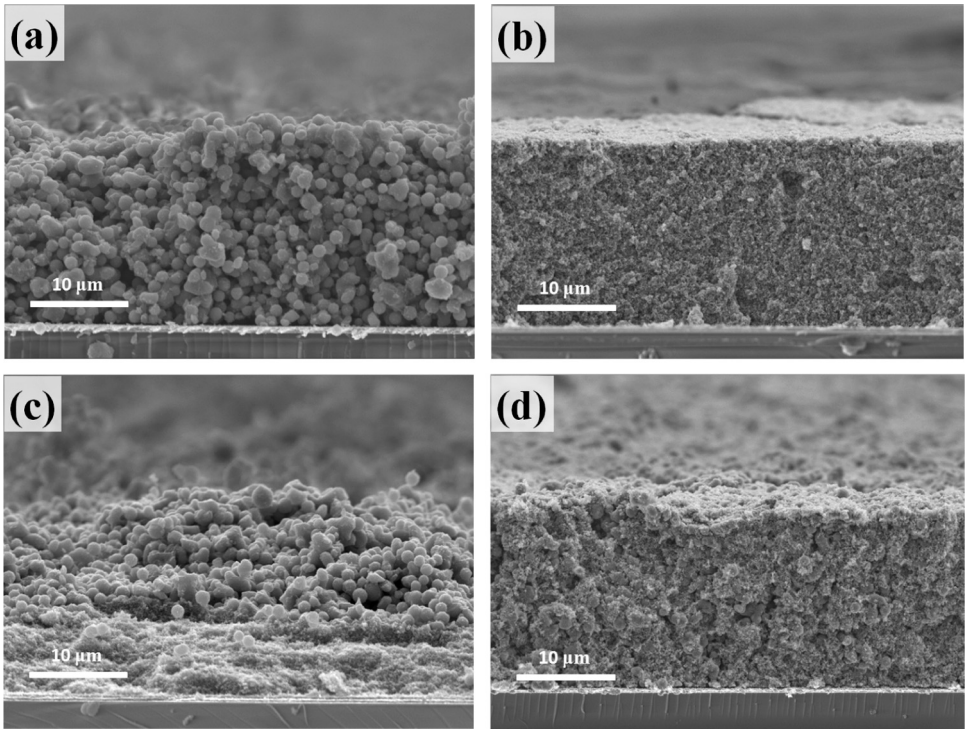

Fig. 4. Cross section SEM images of four photoanode films prepared by (a) a single-layer of mesoporous TiO_2 beads, (b) a single-layer of standard Degussa P25 TiO_2 nanoparticles, (c) a double-layer configuration composed of a ~10 μm beads layer on top of a ~7 μm P25 layer, and (d) a single-layer of the mixture of P25 and beads (weight ratio≈1/1).

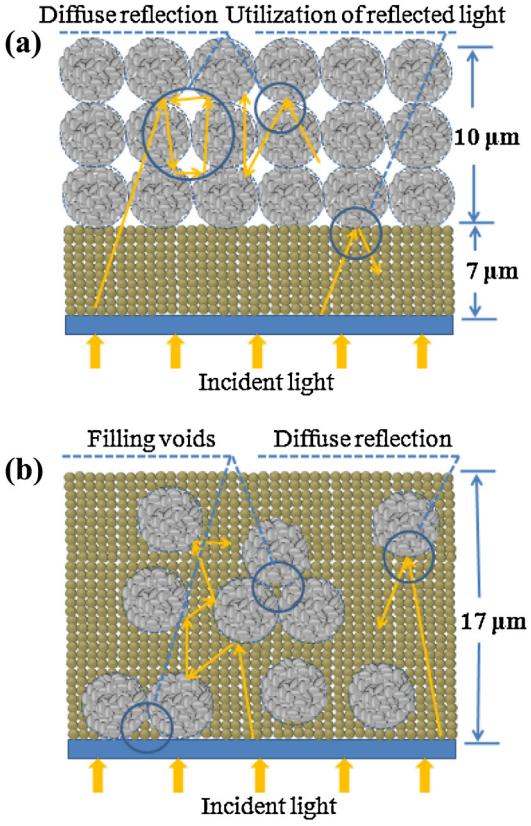

Fig. 5. Schematic drawings showing the benefits of the combined use of mesoporous TiO_2 beads and P25 nanoparticles in two designed photoanodes: (a) double-layer configuration, and (b) mixture configuration.

neighboring beads, as demonstrated by the schematic drawing in Fig. 5b, and thus will further increase the amount of QDs loaded per unit photoanode area without increasing the film thickness. Moreover, such a mixture structure might be conducive for the formation of better connection between the beads and better contact between the TiO_2 film and FTO substrate, and thus improve the electron transport in the photoanode and reduce the charge recombination. The improved double-layer and mixture configurations for the photoanodes as shown in Fig. 4c and d are expected to address the drawbacks in the single-layer films simply consisting of mesoporous beads or P25 nanoparticles and thus improve the performance of QDSCs. In DSCs, the similar double-layer and mixture structures have already been employed and proved to promote the power conversion efficiency. In the work performed by Huang et al. [40] and Yu et al. [43], the highest efficiencies were obtained with double-layer structured photoanodes in which the mesoporous beads film serves as the active layer. Xi et al. achieved the enhanced performance in DSCs with the mixture photoanode configuration made of TiO_2 beads and nanoparticles [42].

Fig. 6 shows the *J-V* curves of the cells assembled from the as-prepared four photoanodes. The open circuit voltage (V_{oc}), short circuit current density (J_{sc}), fill factor (FF), and overall power conversion efficiencies (η) of those QDSCs are collected in Table 2. It was found that the cells made from mesoporous beads and P25 films displayed the power conversion efficiencies of 4.05% and 4.07%,

Table 2
Photovoltaic properties of CdS/CdSe QDs co-sensitized solar cells made from the as-prepared beads, P25, double-layer and mixture photoanodes measured under the illumination of one Sun (AM 1.5, 100 mW/cm^2).

Photoanodes	V_{oc} (V)	J_{sc} (mA/cm^2)	FF	η (%)
Beads [38]	0.54	13.89	0.54	4.05
P25	0.58	13.27	0.53	4.07
Double-layer	0.55	14.85	0.53	4.33
Mixture	0.58	15.14	0.53	4.65

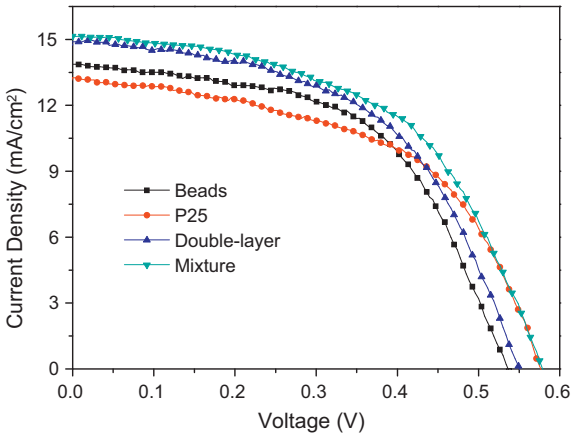

Fig. 6. *J-V* curves for CdS/CdSe QDs co-sensitized solar cells made from the as-prepared beads [38], P25, double-layer and mixture photoanodes measured under the illumination of one Sun (AM 1.5, 100 mW/cm^2).

respectively, exhibiting little difference. However, it is noteworthy that the beads film delivered a J_{sc} of 13.89 mA/cm^2, a little higher than 13.27 mA/cm^2 for P25 film and a V_{oc} of 0.54 V, slightly smaller than 0.58 V for P25 film. The lower V_{oc} for mesoporous beads compared to P25 nanoparticles, might be attributed to the poor connection between the beads and poor contact between the TiO_2 film and FTO substrate, which hindered the electron transport. Although it is believed that the electron transport within a single mesoporous bead should be highly efficient in view of the close attachment of primary nanocrystallites, the drawback of this structure would be the difficulty in the electron transport between neighboring beads due to the small contact area [41]. However, the high QD loading and strong scattering effect of the beads compensated for this drawback and led to a considerable photocurrent and overall power conversion efficiency. Compared to the similar power conversion efficiency obtained here for the QDSCs based on the beads and nanoparticles films, Chen et al. reported a significant higher efficiency (7.20%) for the mesoporous beads as the photoanode in DSCs than that of derived from P25 nanoparticles (5.66%) [31]. This is likely to be associated with some obvious differences between two types of solar cells when porous beads are applied. For example, it may be relatively easy for dye molecules to penetrate into the innermost part of the beads to form full coverage through self-assembly, while QDs are relatively bulky and may have great difficulty to diffuse into the innermost part of the tortuous mesopores, and there is not a strong driving force for QDs to self-assemble to a fully coverage monolayer.

The photoanode with double-layer configuration showed an impressive improvement of the cell performance (4.33%) compared to mesoporous beads film, resulting from an increased J_{sc} of 14.85 mA/cm^2. Such an optimized double-layer structure improved the utilization of incident light compared to the single-layer mesoporous beads and P25 films, and thus gave rise to increased photocurrent. As for the photoanode film prepared from the mixture of mesoporous beads and P25 nanoparticles, a power conversion efficiency as high as 4.65% was achieved, nearly 13% enhancement compared to that of mesoporous beads or P25 films. This can be explained by the effective light scattering of the beads as the scattering centers, increased accessible surface for QD loading and improved electron transport in the photoanode due to the better connection between the neighboring beads, as illustrated in Fig. 5. These results indicate that the combined use of mesoporous beads and P25 nanoparticles for the preparation of photoanodes can significantly improve the cell performance.

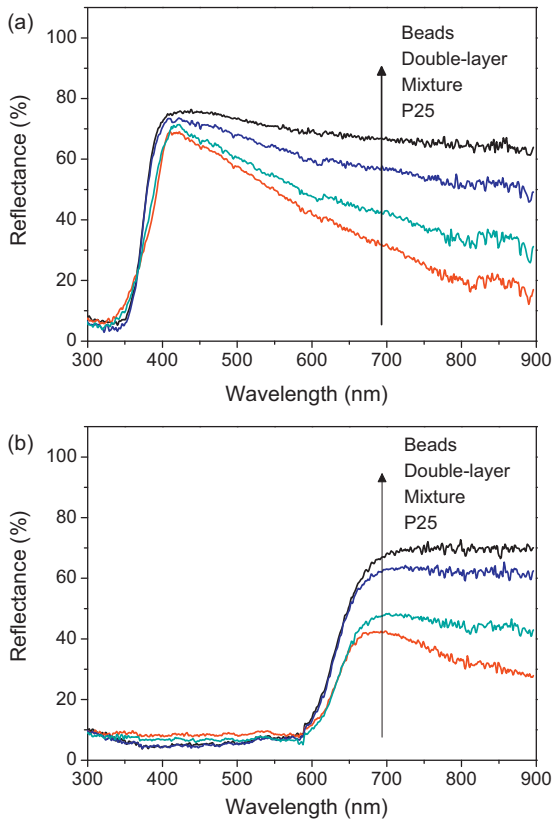

Fig. 7. Diffuse reflectance spectra of the beads [38], P25, double-layer and mixture photoanode films (a) before and (b) after CdS/CdSe QDs sensitization.

Diffuse reflectance spectra of the four TiO_2 photoanode films before and after CdS/CdSe QDs sensitization are shown in Fig. 7, which reflect their different light scattering capabilities. All of the photoanode films before QDs sensitization exhibited high diffuse reflectance in the visible range of 400-500 nm, while a distinctly rapid decline in light scattering was observed for P25 film in the wavelength range from 500 to 900 nm due to the small TiO_2 particle size. In contrast, the film composed of mesoporous TiO_2 beads had higher diffuse reflection capabilities in the visible and near-infrared region, suggesting that the incident light was significantly scattered within the film due to the comparable bead size to the wavelength of visible light. As expected, the diffuse reflectance of the double-layer and mixture films lay between those of beads and P25 films. Mesoporous beads as the upper layer or scattering centers suppressed the transmittance at longer wavelengths. After QDs sensitization, the reflectance spectra followed the same trend, and the remarkable drop over the wavelength ranging from 400 to 650 nm mainly resulted from the strong light absorption by CdS/CdSe QDs.

Fig. 8 shows the Nyquist plots of EIS for QDSCs with four different photoanodes measured under forward bias (-0.6 V) under dark condition. The two semicircles exhibited in the plots corresponded to the impedances of the electron ejection at the counter electrode/electrolyte interface and transport in the electrolyte at high frequencies (R_1, smaller semicircle), and the electron transfer at the TiO_2/QDs/electrolyte interface and transport in the TiO_2 film (R_2, bigger semicircle), respectively [44]. Apparently, the largest R_2 (121.3 Ω, based on the equivalent circuit model) was obtained for P25 film, while the beads film delivered the lowest R_2 (84.7 Ω) among the four photoanodes. As R_2 is commonly considered to be mainly determined by the charge recombination resistance, with partial contribution from transport resistance, large R_2 suggests

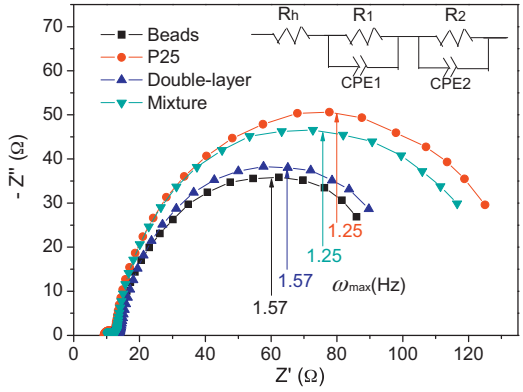

Fig. 8. Nyquist plots of EIS spectra measured under dark condition at an applied forward bias of -0.6 V for the QDSCs made from the as-prepared beads [38], P25, double-layer and mixture photoanodes. Inset displays the corresponding equivalent circuit.

the retarded backward reaction of injected electron transfer at the TiO_2/QD/electrolyte interface, i.e., reduced interfacial recombination [45–47]. However, for the mesoporous beads film, it is conjectured that the formation of QDs adsorbed onto the TiO_2 located in the inner part of the beads might not be as easy as that for the outer part. As the poor QD loading would cause the direct exposure of TiO_2 to the electrolyte, which might be responsible for the comparative low R_2, the beads film exhibited more serious charge recombination compared to P25 film. The charge recombination in the beads film can be suppressed when combined with P25 nanoparticles to prepare the double-layer and mixture photoanodes in consideration of the increased R_2 lies between those of beads and P25 photoanodes, especially for the photoanode with the mixture configuration.

Furthermore, for DSCs, it is generally accepted that a decrease in the frequency at the maximum imaginary resistance of the second semicircle (ω_{max}) in the Nyquist plot is correlated with an increase in V_{oc}, which is due to the retarded backward reaction at open circuit conditions under illumination. The V_{oc} of a DSC can be expressed by the following equation [45,48]:

$$V_{oc} = \frac{RT}{\beta F} \ln\left(\frac{AI}{n_0 k_b [I_3^-] + n_0 k_r [D^+]}\right) \quad (1)$$

where R is the molar gas constant, T is the temperature, F is the Faraday constant, and β is the reaction order for I_3^- and electrons, A is the electrode area, I is the incident photon flux, n_0 is the concentration of accessible electronic states in the conduction band, and k_b and k_r are the kinetic constant of the backreaction of the injected electrons with triiodide and the recombination of these electrons with oxidized dyes (D^+), respectively. For QDSCs, the redox couple is $S^{2-}/S_n{}^{2-}$ instead of I^-/I_3^-. Considering that ω_{max} is the same as the backreaction constant (k_b) [45,49], and that the $S_n{}^{2-}$ in the electrolyte is constant under our experimental conditions, V_{oc} will depend logarithmically on $1/\omega_{max}$ as the loss term $n_0 k_r [D^+]$ can be neglected [45,48]. As displayed in Fig. 8, P25 and the mixture photoanodes delivered a larger ω_{max} compared to the beads and double-layer photoanodes. Therefore, according to Eq. (1), the larger V_{oc} of QDSC employing P25 and mixture photoanodes could be obtained, which was consistent with the results obtained from *J-V* curves.

4. Conclusions

Submicrometer-sized mesoporous TiO_2 beads combined with TiO_2 nanoparticles offer unique advantages as photoanodes for QDSC application: mesoporous TiO_2 beads possess notably high specific surface area for high QD loading and effective light scattering giving rise to enhanced light harvesting; the incorporation of individually dispersed TiO_2 nanoparticles into the large voids between submicrometer-sized beads would lead to increased accessible surface for QD loading, better connection between the neighboring beads and retarded charge recombination in the photoanode. The unique hierarchical pore structure of the beads would also facilitate electrolyte diffusion. Double-layer and mixture configurations were developed, in order to optimize the photoanode structure to reach the requirements of high QD loading, strong light scattering, efficient electron transport and quick electrolyte diffusion. Photovoltaic characteristics revealed that the photoanodes of double-layer and mixture configuration really delivered marked improvements (4.33% and 4.65%) in the cell performance, compared with the simple single-layer beads or nanoparticle films (4.05% and 4.07%). The as-prepared mesoporous TiO_2 bead structure offers great potential for the development of high efficiency QDSCs.

Acknowledgements

This work was supported in part by the National Science Foundation (DMR 1035196), the University of Washington TGIF grant, and the Royalty Research Fund (RRF) from the Office of Research at the University of Washington. Ru Zhou would also like to acknowledge the fellowship from China Scholarship Council.

References

[1] M. Graetzel, R.A.J. Janssen, D.B. Mitzi, E.H. Sargent, Materials interface engineering for solution-processed photovoltaics, Nature 488 (2012) 304.
[2] P.K. Santra, P.V. Kamat, Mn-doped quantum dot sensitized solar cells: a strategy to boost efficiency over 5%, Journal of the American Chemical Society 134 (2012) 2508.
[3] M.A. Hossain, J.R. Jennings, Z.Y. Koh, Q. Wang, Carrier generation and collection in CdS/CdSe-sensitized SnO_2 solar cells exhibiting unprecedented photocurrent densities, ACS Nano 5 (2011) 3172.
[4] J. Ryu, S.H. Lee, D.H. Nam, C.B. Park, Rational design and engineering of quantum-dot-sensitized TiO_2 nanotube arrays for artificial photosynthesis, Advanced Materials 23 (2011) 1883.
[5] T. Sugaya, O. Numakami, R. Oshima, S. Furue, H. Komaki, T. Amano, K. Matsubara, Y. Okano, S. Niki, Ultra-high stacks of InGaAs/GaAs quantum dots for high efficiency solar cells, Energy & Environmental Science 5 (2012) 6233.
[6] P.V. Kamat, Quantum dot solar cells. Semiconductor nanocrystals as light harvesters, Journal of Physical Chemistry C 112 (2008) 18737.
[7] V. Gonzalez-Pedro, X. Xu, I. Mora-Sero, J. Bisquert, Modeling high-efficiency quantum dot sensitized solar cells, ACS Nano 4 (2010) 5783.
[8] G. Zhu, L. Pan, T. Xu, Z. Sun, CdS/CdSe-cosensitized TiO_2 photoanode for quantum-dot-sensitized solar cells by a microwave-assisted chemical bath deposition method, ACS Applied Materials & Interfaces 3 (2011) 3146.
[9] J.J. Tian, Q.F. Zhang, E. Uchaker, Z.Q. Liang, R. Gao, X.H. Qu, S.G. Zhang, G.Z. Cao, Constructing ZnO nanorod array photoelectrodes for highly efficient quantum dot sensitized solar cells, Journal of Materials Chemistry A 1 (2013) 6770.
[10] J.J. Tian, Q.F. Zhang, L.L. Zhang, R. Gao, L.F. Shen, S.G. Zhang, X.H. Qu, G.Z. Cao, ZnO/TiO_2 nanocable structured photoelectrodes for CdS/CdSe quantum dot co-sensitized solar cells, Nanoscale 5 (2013) 936.
[11] J.J. Tian, Q.F. Zhang, E. Uchaker, R. Gao, X.H. Qu, S.G. Zhang, G.Z. Cao, Architectured ZnO photoelectrode for high efficiency quantum dot sensitized solar cells, Energy & Environmental Science 6 (2013) 3542.
[12] O.E. Semonin, J.M. Luther, S. Choi, H.-Y. Chen, J.B. Gao, A.J. Nozik, M.C. Beard, Peak external photocurrent quantum efficiency exceeding 100% via MEG in a quantum qot solar cell, Science 334 (2011) 1530.
[13] Y. Tak, S.J. Hong, J.S. Lee, K. Yong, Fabrication of ZnO/CdS core/shell nanowire arrays for efficient solar energy conversion, Journal of Materials Chemistry 19 (2009) 5945.
[14] J. Kim, H. Choi, C. Nahm, J. Moon, C. Kim, S. Nam, D.R. Jung, B. Park, The effect of a blocking layer on the photovoltaic performance in CdS quantum-dot-sensitized solar cells, Journal of Power Sources 196 (2011) 10526.
[15] I. Robel, V. Subramanian, M. Kuno, P.V. Kamat, Quantum dot solar cells. Harvesting light energy with CdSe nanocrystals molecularly linked to mesoscopic TiO_2 films, Journal of the American Chemical Society 128 (2006) 2385.
[16] M. Samadpour, S. Giménez, P.P. Boix, Q. Shen, M.E. Calvo, N. Taghavinia, A.I. zad, T. Toyoda, H. Míguez, I. Mora-Seró, Effect of nanostructured electrode architecture and semiconductor deposition strategy on the photovoltaic performance of quantum dot sensitized solar cells, Electrochimica Acta 75 (2012) 139.

[17] Z. Yang, H.–T. Chang, CdHgTe and CdTe quantum dot solar cells displaying an energy conversion efficiency exceeding 2%, Solar Energy Materials and Solar Cells 94 (2010) 2046.
[18] A. Braga, S. Giménez, I. Concina, A. Vomiero, I. Mora-Sero, Panchromatic sensitized solar cells based on metal sulfide quantum dots grown directly on nanostructured TiO_2 electrodes, Journal Physical Chemistry Letters 2 (2011) 454.
[19] A. Tubtimtae, K.L. Wu, H.Y. Tung, M.W. Lee, G.J. Wang, Ag_2S quantum dot-sensitized solar cells, Electrochemistry Communications 12 (2010) 1158.
[20] J. Burschka, N. Pellet, S.-Jin. Moon, R. Humphry-Baker, P. Gao, M.K. Nazeeruddin, M. Grätzel, Sequential deposition as a route to high-performance perovskite-sensitized solar cells, Nature 499 (2013) 316.
[21] Q.F. Zhang, K. Park, J.T. Xi, D. Myers, G.Z. Cao, Recent progress in dye-sensitized solar cells using nanocrystallite aggregates, Advanced Energy Materials 1 (2011) 988.
[22] Y.L. Lee, Y.S. Lo, Highly efficient quantum-qot-sensitized solar cell based on co-sensitization of CdS/CdSe, Advanced Functional Materials 19 (2009) 604.
[23] B. Oregan, M. Grätzel, A low-cost, high-efficiency solar-cell based on dye-sensitized colloidal TiO_2 films, Nature 353 (1991) 737.
[24] A. Yella, H.W. Lee, H.N. Tsao, C.Y. Yi, A.K. Chandiran, M.K. Nazeeruddin, E.W.G. Diau, C.Y. Yeh, S.M. Zakeeruddin, M. Grätzel, Porphyrin-sensitized solar cells with cobalt (II/III)–based redox electrolyte exceed 12 percent efficiency, Science 334 (2011) 629.
[25] M. Grätzel, Solar energy conversion by dye-sensitized photovoltaic cells, Inorganic Chemistry 44 (2005) 6841.
[26] S. Ito, P. Chen, P. Comte, M.K. Nazeeruddin, P. Liska, P. Pechy, M. Grätzel, Fabrication of screen-printing pastes from TiO_2 powders for dye-sensitised solar cells, Progress in Photovoltaics 15 (2007) 603.
[27] H.C. van de Hulst, Light Scattering by Small Particles, Wiley, New York, 1957.
[28] P.E. Wolf, G. Maret, Weak localization and coherent backscattering of photons in disordered media, Physical Review Letters 55 (1985) 2696.
[29] Q.F. Zhang, T.R. Chou, B. Russo, S.A. Jenekhe, G.Z. Cao, Aggregation of ZnO nanocrystallites for high conversion efficiency in dye-sensitized solar cells, Angewandte Chemie International Edition 47 (2008) 2402.
[30] Q.F. Zhang, T.R. Chou, B. Russo, S.A. Jenekhe, G.Z. Cao, Polydisperse aggregates of ZnO nanocrystallites: a method for energy-conversion-efficiency enhancement in dye-sensitized solar cells, Advanced Functional Materials 18 (2008) 1654.
[31] D.H. Chen, F.Z. Huang, Y.-B. Cheng, R.A. Caruso, Mesoporous anatase TiO_2 beads with high surface areas and controllable pore sizes: a superior candidate for high-performance dye-sensitized solar cells, Advanced Materials 21 (2009) 2206.
[32] J. Ferber, J. Luther, Computer simulations of light scattering and absorption in dye-sensitized solar cells, Solar Energy Materials and Solar Cells 54 (1998) 265.
[33] Z.-S. Wang, H. Kawauchi, T. Kashima, H. Arakawa, Significant influence of TiO_2 photoelectrode morphology on the energy conversion efficiency of N719 dye-sensitized solar cell, Coordination Chemistry Reviews 248 (2004) 1381.
[34] S. Ito, M.K. Nazeeruddin, S.M. Zakeeruddin, P. Pechy, P. Comte, M. Grätzel, T. Mizuno, A. Tanaka, T. Koyanagi, Study of dye-sensitized solar cells by scanning electron micrograph observation and thickness optimization of porous TiO_2 electrodes, International Journal of Photoenergy 2009 (2009) 517609.
[35] S. Ito, T.N. Murakami, P. Comte, P. Liska, C. Grätzel, M.K. Nazeeruddin, M. Grätzel, Fabrication of thin film dye sensitized solar cells with solar to electric power conversion efficiency over 10%, Thin Solid Films 516 (2008) 4613.
[36] Q. Wang, S. Ito, M. Grätzel, F. Fabregat-Santiago, I. Mora-Seró, J. Bisquert, T. Bessho, H. Imai, Characteristics of high efficiency dye-sensitized solar cells, Journal of Physical Chemistry B 110 (2006) 25210.
[37] S. Hore, C. Vetter, R. Kern, H. Smit, A. Hinsch, Influence of scattering layers on efficiency of dye-sensitized solar cells, Solar Energy Materials and Solar Cells 90 (2006) 1176.
[38] R. Zhou, Q.F. Zhang, E. Uchaker, J.L. Lan, M. Yin, G.Z. Cao, Mesoporous TiO_2 beads for high efficiency CdS/CdSe quantum dot co-sensitized solar cells, Journal of Materials Chemistry A 2 (2014) 2517.
[39] D.H. Chen, L. Cao, F.Z. Huang, P. Imperia, Y.-B. Cheng, R.A. Caruso, Synthesis of monodisperse mesoporous titania beads with controllable diameter, high surface areas, and variable pore diameters (14-23 nm), Journal of the American Chemical Society 132 (2010) 4438.
[40] F.Z. Huang, D.H. Chen, X.L. Zhang, R.A. Caruso, Y.-B. Cheng, Dual-function scattering layer of submicrometer-sized mesoporous TiO_2 beads for high-efficiency dye-sensitized solar cells, Advanced Functional Materials 20 (2010) 1301.
[41] Y.J. Kim, M.H. Lee, H.J. Kim, G. Lim, Y.S. Choi, N.G. Park, K. Kim, W.I. Lee, Formation of highly efficient dye-sensitized solar cells by hierarchical pore generation with nanoporous TiO_2 spheres, Advanced Materials 21 (2009) 3668.
[42] J.T. Xi, Q.F. Zhang, K. Park, Y.M. Sun, G.Z. Cao, Enhanced power conversion efficiency in dye-sensitized solar cells with TiO_2 aggregates/nanocrystallites mixed photoelectrodes, Electrochimica Acta 56 (2011) 1960.
[43] I.G. Yu, Y.J. Kim, H.J. Kim, C. Lee, W.I. Lee, Size-dependent light-scattering effects of nanoporous TiO_2 spheres in dye-sensitized solar cells, Journal of Materials Chemistry 21 (2011) 532.
[44] N. Koide, A. Islam, Y. Chiba, L.Y. Han, Improvement of efficiency of dye-sensitized solar cells based on analysis of equivalent circuit, Journal of Photochemistry and Photobiology A: Chemistry 182 (2006) 296.
[45] K. Lee, S.W. Park, M.J. Ko, K. Kim, N.-G. Park, Selective positioning of organic dyes in a mesoporous inorganic oxide film, Nature Materials 8 (2009) 665.
[46] R. Kern, R. Sastrawan, J. Ferber, R. Stangl, J. Luther, Modeling and interpretation of electrical impedance spectra of dye solar cells operated under open-circuit conditions, Electrochimica Acta 47 (2002) 4213.
[47] J.V.D. Lagemaat, N.G. Park, A.J. Frank, Influence of electrical potential distribution, charge transport, and recombination on the photopotential and photocurrent conversion efficiency of dye-sensitized nanocrystalline TiO_2 solar cells: a study by electrical impedance and optical modulation techniques, Journal of Physical Chemistry B 104 (2000) 2044.
[48] Q. Wang, J.-E. Moser, M. Grätzel, Electrochemical impedance spectroscopic analysis of dye-sensitized solar cells, Journal of Physical Chemistry B 109 (2005) 14945.
[49] M. Adachi, M. Sakamoto, J. Jiu, Y. Ogata, S. Isoda, Determination of parameters of electron transport in dye-sensitized solar cells using electrochemical impedance spectroscopy, Journal of Physical Chemistry B 110 (2006) 13872.